IPCC climate models do not capture Arctic sea ice drift acceleration: Consequences in terms of projected sea ice thinning and decline

P. Rampal, Jérôme Weiss, C. Dubois, J.-M. Campin

IPCC climate models do not capture Arctic sea ice drift acceleration: Consequences in terms of projected sea ice thinning and decline

P. Rampal,[1,2] J. Weiss,[2] C. Dubois,[3] and J.-M. Campin[1]

Received 7 March 2011; revised 22 June 2011; accepted 30 June 2011; published 29 September 2011.

[1] IPCC climate models underestimate the decrease of the Arctic sea ice extent. The recent Arctic sea ice decline is also characterized by a rapid thinning and by an increase of sea ice kinematics (velocities and deformation rates), with both processes being coupled through positive feedbacks. In this study we show that IPCC climate models underestimate the observed thinning trend by a factor of almost 4 on average and fail to capture the associated accelerated motion. The coupling between the ice state (thickness and concentration) and ice velocity is unexpectedly weak in most models. In particular, sea ice drifts faster during the months when it is thick and packed than when it is thin, contrary to what is observed; also models with larger long-term thinning trends do not show higher drift acceleration. This weak coupling behavior (1) suggests that the positive feedbacks mentioned above are underestimated and (2) can partly explain the models' underestimation of the recent sea ice area, thickness, and velocity trends. Due partly to this weak coupling, ice export does not play an important role in the simulated negative balance of Arctic sea ice mass between 1950 and 2050. If we assume a positive trend on ice speeds at straits equivalent to the one observed since 1979 within the Arctic basin, first-order estimations give shrinking and thinning trends that become significantly closer to the observations.

Citation: Rampal, P., J. Weiss, C. Dubois, and J.-M. Campin (2011), IPCC climate models do not capture Arctic sea ice drift acceleration: Consequences in terms of projected sea ice thinning and decline, *J. Geophys. Res.*, *116*, C00D07, doi:10.1029/2011JC007110.

1. Introduction

[2] There is now significant evidence of shrinking of the Arctic sea ice extent during the last decades [*Lemke et al.*, 2007; *Serreze et al.*, 2007], with a significant acceleration of this decline within the last few years [*Comiso et al.*, 2008]. As a result of this shrinkage, the ice albedo positive feedback over the Arctic Ocean during summer can have an increasing role in warming of northern latitudes and possibly of the entire planet (see, e.g., *Serreze and Francis* [2006] about Arctic amplification). In comparison with observations, climate models underestimate this decline [*Stroeve et al.*, 2007] and its recent acceleration is in general mostly unforeseen [*Serreze*, 2009]. This systematic underestimation gives rise to questions about the Arctic sea ice coverage and climate projections for the XXIst century both at the regional and global scale.

[3] Owing to the complexity of the Arctic basin as a physical system involving many interacting processes and feedbacks (negative or positive), several explanations have been proposed to explain the models deficiencies. These can be separated into two main categories: those involving mechanical processes and those involving thermodynamic processes. Within this second category are, for example, (1) a too weak albedo positive feedback that is expressed in models by the linear relationships between polar and global temperatures and between polar temperature and albedo, and that results in the underestimation of the Arctic amplification [*Winton*, 2008], (2) an excessive negative feedback in winter caused by a too strong temperature inversion [*Boé et al.*, 2009a], and (3) a too simplified parameterization of the ice albedo [*Stroeve et al.*, 2007] that contributes to the underestimation of ice melting through, e.g., melt pond formation [*Skyllingstad et al.*, 2009]. Polar clouds, which are known to have an important impact on the shortwave and longwave radiative budget of the Arctic ocean and so on sea ice mass balance [*Gorodetskaya et al.*, 2008], remain also a large source of uncertainty in climate models [e.g., *Eisenman et al.*, 2007; *Vavrus et al.*, 2009].

[4] Mechanical-related processes can be another source of deficiency in models. As an example, a poor representation of the modes of atmospheric variability such as the North

[1]Earth, Atmospheric and Planetary Science, Massachusetts Institute of Technology, Cambridge, Massachusetts, USA.
[2]Laboratoire de Glaciologie et Géophysique de l'Environnement, CNRS/Université Joseph Fourier, St Martin d'Hères, France.
[3]Centre National de Recherches Météorologiques, Toulouse, France.

0148-0227/11/2011JC007110

Table 1. IPCC AR4 Model IDs and the Principal Characteristics of the Corresponding Sea Ice Models[a]

Model ID	Number of Runs Analyzed	Velocity Grid Resolution		Resolution (Number of Points)	Rheology	ITD	Ice Thickness Categories	Ice Layers
		Latitude	Longitude					
BCCR-BCM2.0	1	0,5°	1°	3612	VP	No	1	1
CNRM-CM3	1	1°	2°	1809	EVP	Yes	4	4
GISS aom	2	3°	4°	311	cavitating fluid	No	1	4
GISS er	5	4°	2.5°	147	VP	No	1	4
FGOALS-g1.0	1	1°	1°	3786	EVP	Yes	5	16
INGV-SXG	1	1°	1°	3612	VP	No	1	2
INM-CM3.0	1	2°	2.5°	1440	no dynamics	No	1	1
MIROC3.2(Hires)	1	0.56°	1.125°	3576	EVP	No	1	1
MIUB-ECHO-G	3	2.8°	2.8°	433	VP	No	1	1
ECHAM5/MPI-OM	2	1°	1°	3616	VP	No	1	1
MRI-CGCM2.3.2	5	2°	2.5°	727	none: perfect fluid	No	1	1
NCAR ccsm-PCM	5	0.53°	1.125°	3581	EVP	Yes	5	4
UKMO-HadGEM1	1	1.25°	1.25°	2163	EVP	Yes	5	1
Total	28							

[a]The number of ice thickness categories is that considered in the ITD scheme (1 category if no ITD). The number of ice layers is that considered in the thermodynamics sea ice model. The resolution is given as the number of grid points of the sea ice model over the central Arctic basin (region outlined by *Rampal et al.* [2009, Figure 1]).

Atlantic Oscillation (NAO) or the Arctic Oscillation (AO) [*Stroeve et al.*, 2007] can impact the Transpolar drift as well as ice export through Fram Strait [*Kwok et al.*, 2004; *Nghiem et al.*, 2007]. Upper ocean circulation, which acts on the ice cover as an important mechanical forcing, is often poorly represented [e.g., *Tremblay et al.*, 2007]. An inaccurate representation of sea-ice kinematics may also be an important shortcoming for reproducing the current sea ice decline.

[5] Sea ice state and kinematics have been associated with profound changes in recent decades. Arctic sea ice shrinkage is accompanied by a strong thinning seen in ice draft as well as ICESat ice freeboard data. Between 1980 and 2008 the net average mean thickness has decreased by 1.75 m in winter and 1.65 m in summer [*Kwok and Rothrock*, 2009]. Taking into account the thickness uncertainties, this average thinning corresponds to a trend of 16.5(±7.0)% per decade over the same period, which can be essentially explained by a drastic reduction of the perennial ice cover [*Kwok et al.*, 2009]. At the same time, Arctic sea ice kinematics have undergone large changes [*Hakkinen et al.*, 2008; *Rampal et al.*, 2009]. From buoy data, *Rampal et al.* [2009] showed that the sea ice drift speed has increased at a rate of 9.0(±1.9)% per decade on average within the Arctic basin from 1979 to 2007, whereas the average deformation rate has increased at a rate larger than 50(±10)% per decade over the same period.

[6] These recent and simultaneous changes in sea ice state, deformation and drift are likely intimately coupled in the following way: Increasing deformation implies stronger fracturing, hence more lead opening and a decreasing albedo [*Zhang et al.*, 2000]. This, in turn, favors sea ice thinning in the summer and delays refreezing in early winter, i.e., strengthen sea ice decline. Note however that a negative feedback between sea ice fracturing and sea ice shrinking can also occur in winter, when the thermodynamically driven production of new ice is enhanced along newly open leads. Ice thinning results in decreased mechanical strength and therefore allows more fracturing, hence larger drifting speed and deformation rates. In turn, this could accelerate the export of sea ice through Fram Strait with a significant impact on sea ice mass balance [*Haas et al.*, 2008; *Rampal et al.*, 2009]. Similarly, sea ice mechanical weakening decreases the likelihood of arch formation along Nares Strait, therefore allowing old, thick ice to be exported through this strait [*Kwok et al.*, 2010]. Finally, accelerated drift and deformation most likely imply that sea ice remains on average a shorter time within the basin; that is, the average ice age [*Maslanik et al.*, 2007; *Tschudi et al.*, 2010] and ice thickness decrease.

[7] Consequently, the quality of the future projections of the sea ice cover, of the Arctic climate, and beyond, partly relies on the ability of climate models to properly simulate the respective observed sea-ice area, thickness and drift trends, as well as the positive feedbacks described above. In this study, we evaluate these trends for the models of the International Panel on Climate Change Fourth Assessment Report (IPCC AR4) and show that they (1) strongly underestimate the Arctic sea ice thinning observed during the last decades and (2) do not capture the concomitant sea ice drift acceleration. Then we discuss the role that an unexpectedly weak coupling between the simulated ice thickness and velocity may play on these deficiencies, and more specifically of the associated absence of effect of sea ice kinematics trends on the recent sea ice decline. To partly test this hypothesis, we estimate at the first order what the simulated sea ice area and thickness trends would become in case of a sea-ice drift acceleration similar to that observed.

2. Data and Models

[8] We used the IPCC AR4 simulations available from the CMIP3 multimodel data set (http://www-pcmdi.llnl.gov/about/index.php) that deliver monthly averaged sea ice area, thickness and, with the exception of one model without sea ice dynamics (INM-CM3.0), monthly averaged velocity fields. This represents 13 different models and 29 simulations, with varying resolutions and sea ice models and/or parameterizations (Table 1). In each case, monthly time series were reconstructed over the period 1950–2050 from a

combination of the Climate of the 20th Century experiment (20C3M, up to 1999) and the SRES A1B experiment (from 2000) that takes the end of the 20C3M run as its initial condition. Speed values are calculated as the norm of the velocity vectors. Monthly values of thickness and ice speed were spatially averaged to allow a direct comparison with observations. For thickness, spatial averaging was performed over a polygonal region (the so-called "SCICEX box") encompassing most of the submarine tracks [see *Rothrock et al.*, 2008, Figure 2], whereas sea ice speeds were averaged over a larger region covering most of the Arctic basin, north of Bering and Fram Straits and 150 km away from the coastlines (see the "Central Arctic" region of *Rampal et al.* [2009, Figure 1]).

[9] Sea ice physics and rheology varies from one model to another (Table 1). One model (INM-CM3.0) has no sea ice dynamics; that is, thickness variations are only related to thermodynamics. One model (MRI-CGCM2.3.2) has sea ice dynamics but no rheology, i.e., sea ice is treated as a perfect fluid and is simply advected by a function of ocean surface current; it has no viscosity or internal stress. Another model (GISS aom) is based on the cavitating fluid scheme [*Flato and Hibler*, 1992] that allows sea ice to resist convergence, but not divergence or shear. All other models are based on the classical viscous-plastic (VP) rheology [*Hibler*, 1979], in which sea ice has strength under convergence and shear, but offers no resistance to divergence. For stress states inside the plastic yield curve, the mechanical behavior is that of a viscous fluid, while the ice flows as a perfect plastic once the stress state reaches the yield curve. While in the original VP scheme [*Hibler*, 1979] the momentum equation is solved implicitly, some models introduce a nonphysical elastic term to solve it explicitly (elastic-viscous-plastic, listed as EVP in Table 1) [*Hunke and Dukowicz*, 1997]. This, however, does not change the physics of the model (For more details about sea ice rheological and dynamical models, see, e.g., *Feltham* [2008]). A coupling between the ice state (thickness and concentration) and kinematics is expected to take place through the acceleration term in the momentum equation that depends on the ice mass per unit area, and through the ice strength P that defines the size of the yield envelope, when considered. Majority of models use a linear dependence of P on thickness h and an exponential dependence on concentration C, $P \sim h\, e^{-c(1-C)}$, where $c = 20$ [*Hibler*, 1979], which means that ice is almost in free drift for $C < 0.9$. A few models introduce a more sophisticated ice thickness distribution scheme (ITD in Table 1) that allows the coupling of the ice thickness evolution and strength with the dynamics through ridging and rafting mechanisms [*Lipscomb et al.*, 2007; *Salas Mélia*, 2002]. In this case, P scales as $h^{3/2}$, i.e., is more sensitive to thickness than in the classical scheme [*Lipscomb et al.*, 2007].

3. Results

3.1. Thickness

[10] The 12 month running means of the modeled thicknesses fall in the correct order of magnitude (ensemble mean $\approx$ 2 m in 2000), with a standard deviation between simulations of ±0.7 m (Figure 1), except for one model (FGOALS-g1.0) that gives unrealistically large thicknesses of about 8 m on average (not shown on Figure 1). The model without sea ice dynamics (INM-CM3.0) shows the lowest average thicknesses (~0.5 m), far below the observations. This might be related to an absence of deformation-induced redistribution of thin ice into thicker (ridged) ice and of the simultaneous creation of open water areas where new ice can form in winter.

[11] The seasonal cycle is correctly reproduced, with a phase lag less than a month compared to the observations of *Rothrock et al.* [2008], expect for INGV-SXG (2 months of negative phase lag) (Figure 2). However, focusing on the thinning trend over the period 1980 to 2008, the disagreement between models and observations is dramatic (Figure 1): although nearly all simulations show a statistically significant thinning trend over the period (at a 95% confidence level), the ensemble mean trend of −4.6(±1.9)% per decade is almost 4 times smaller than the observed trend of 16.5(±7)% per decade estimated from submarine and ICESat thickness data (Table 2). The strong thinning observed in recent years from ICESat data is particularly poorly forecast (red line + circles of Figure 1). No correlation exists between the sophistication of the sea ice dynamics model, i.e., of the coupling between sea ice dynamics and thickness, and the modeled thinning trend. In particular, INM-CM3.0, for which the thinning results only from thermodynamics, shows a trend of −3.5% per decade. It is well within the models variability, though slightly lower than the ensemble mean. On the other hand, a modest but statistically significant positive correlation exists between the amplitude of this thinning trend and the resolution of the model, defined as the number of grid point over the Arctic (R = 0.56). *Sewall* [2008], who reported a similar resolution influence, argued that it depends more on ocean model resolution and its role on ocean heat transport into the Arctic basin than on the sea ice model resolution per se.

[12] In summary, IPCC AR4 models strongly underestimate Arctic sea ice thinning, in a way even more spectacular than they do for the extent decline [*Stroeve et al.*, 2007]. As the observed thinning is essentially the result of a reduction of the perennial sea ice cover [*Kwok et al.*, 2009; *Nghiem et al.*, 2007], one may wonder to what extent this underestimation of the thinning would simply result from the underestimation of the perennial decline. It was shown that, in terms of summer minimum extent and declining trend, recent years are about 30 to 40 years ahead of the ensemble mean forecast [*Stroeve et al.*, 2007]. We therefore calculated the modeled thinning trends over the period 2020–2050, and found a larger ensemble mean of −9.8(±5.1)% per decade, partly due to a smaller initial thickness in 2020 compared to 1980, but still much lower (in absolute value) than the observed trend. It is consistent with the fact that perennial (i.e., September) modeled sea ice thickness does not thin significantly faster compared to the 12 month running mean thickness (Table 2). This reinforces the hypothesis that models do not capture correctly all the processes leading to this drastic sea ice thinning.

3.2. Drift Acceleration

[13] Most models underestimate by half on average the mean sea ice speed estimated from buoy data (Figure 3). Two particularly poor outliers are FGOALS-g1.0, most probably as the result of unrealistic thicknesses (see above), and MRI-CGCM2.3.2, which has no sea ice rheology.

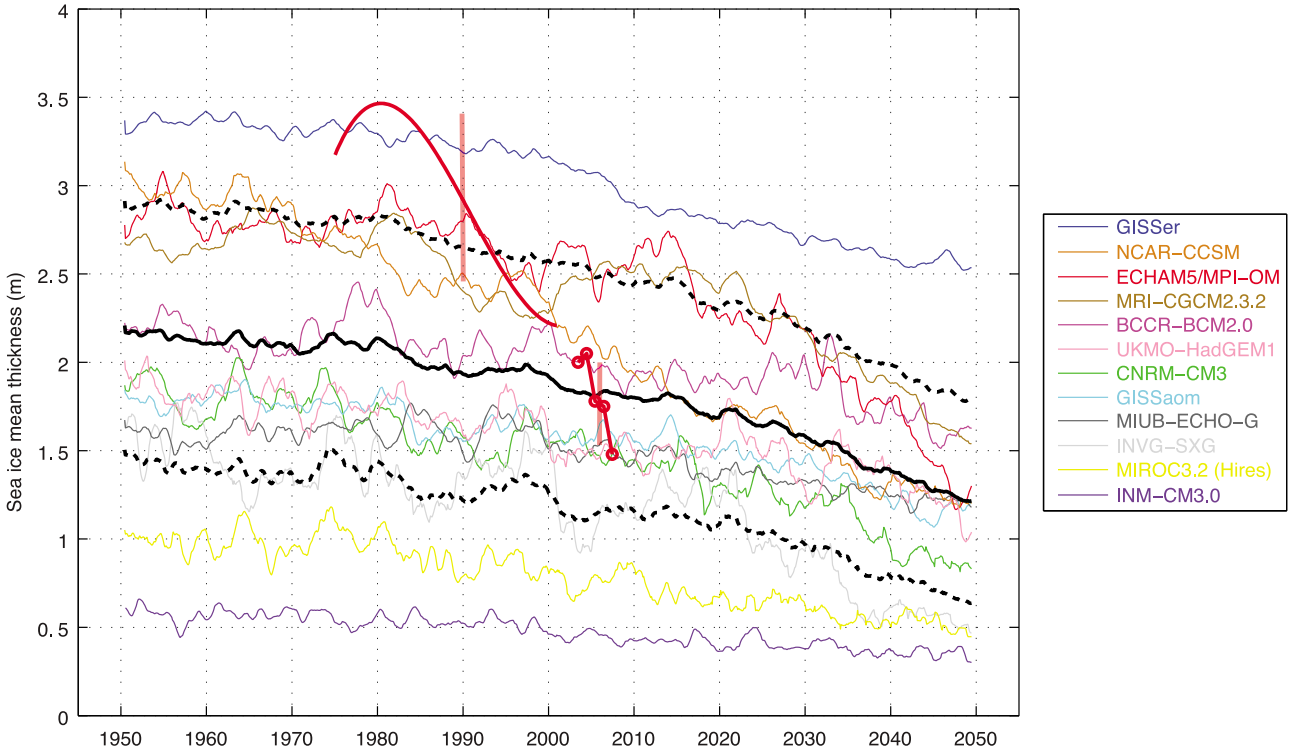

Figure 1. Simulated sea ice mean thicknesses from 1950 to 2050: comparison with observations. Thin colored lines, 12 month running mean of simulated sea ice thicknesses spatially averaged over the polygonal region (so-called SCICEX box) detailed by *Rothrock et al.* [2008]. The FGOALS-g1.0 simulation, which gives unrealistically large thicknesses, is not represented. Only one simulation per model is shown for clarity. Black solid line, ensemble mean. Dashed black lines, ensemble mean ± one standard deviation. Thick red solid line, annually averaged thickness estimated from submarine data, over the SCICEX box region [from *Rothrock et al.*, 2008, equation 9] from 1975 to 2000. Red line + circles, annually averaged thickness estimated from ICESat data over the SCICEX box region for the years 2003 to 2008, and calculated as the mean of winter and summer values reported by *Kwok and Rothrock* [2009]. Light red error bars show residuals in the regression of *Rothrock et al.* [2008] data and quality of ICESat data.

[14] Considering now the normalized sea ice speed trends (in %) over the period 1979–2007, we obtained a large dispersion of values among models, as well as, for a given model, among the different runs (Figure 3 and Table 2). Some trends are negative, i.e., a deceleration, whereas two models, FGOALS-g1.0 and GISS er (run #5), show positive trends similar to the observations, with however unrealistic thicknesses and/or much larger uncertainty. The ensemble mean trend show a positive, but statistically insignificant value of 1.6 ± 1.9% per decade (1.4 ± 2.0% with the FGOALS-g1.0 simulation excluded). This means that IPCC AR4 models do not capture, or at least strongly underestimate, the acceleration of sea ice drift in recent decades. This deficiency unlikely results from resolution limitations, as we found no correlation between the model resolutions and the associated speed trends (R = 0.08). However, this would require confirmation from single model test at different resolutions.

4. Discussion

4.1. Coupling Between Ice State and Kinematics

[15] According to the smaller-than-observed (but nevertheless significant) simulated trends in sea ice extent [*Stroeve et al.*, 2007] and thickness (this study) over the period, and considering the coupling between the ice state (thickness and concentration) and kinematics that theoretically exists in the rheological models, one may have expect a clearer evolution for sea ice drift.

[16] Considering the projected speed trends over the period 2020–2050, which corresponds to summer minimum extents and negative extent trends similar to current observations, we obtained an ensemble mean of 1.6(±1.7)% per decade, i.e., a similar (and still insignificant) value to that of the period 1979–2007. This shows that the delay of models in reproducing an ice cover with a mean thickness close to the current observations cannot explain the incapacity of models to reproduce the associated ice speed trend. This reinforces the fact that the coupling between ice state and ice kinematics in current climate models is very weak. This is confirmed by (1) an absence of correlation between the sophistication of the rheological model and the simulated speed trend and (2) a lack of correlation between simulated thickness and speed trends (R = 0.003), i.e., models that thin faster do not necessarily accelerate more.

[17] A further confirmation is given by the analysis of the speed annual cycle. A very clear seasonal cycle with a minimum speed in March and a maximum speed in September was obtained from buoy drift data [*Rampal et al.*, 2009],

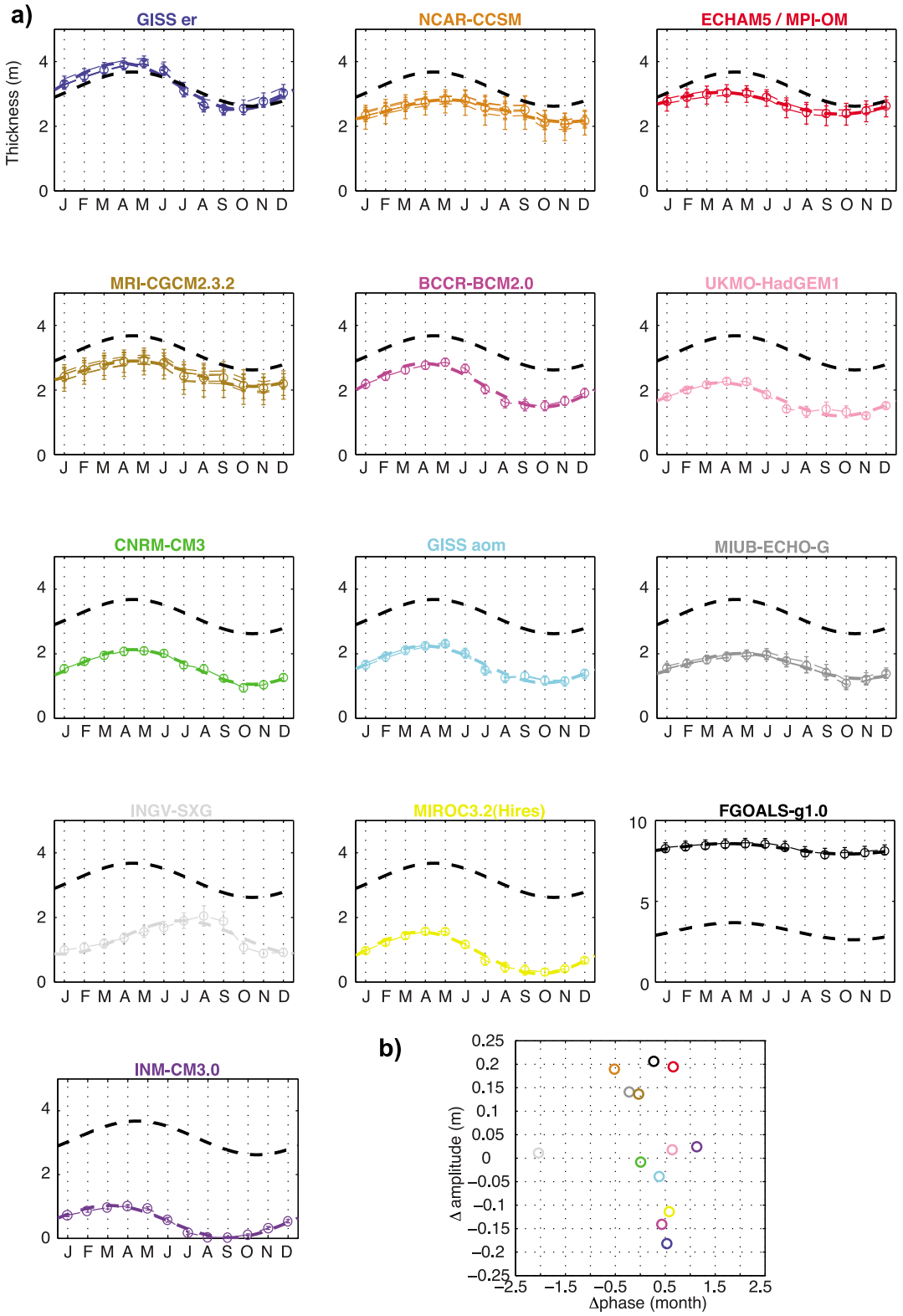

Figure 2. Annual cycle of spatially averaged thickness. (a) Comparison of the simulated sea ice thickness annual cycles with the cycle estimated from submarine data over the period 1975–2000 by *Rothrock et al.* [2008], in dashed black line. Accordingly, the simulated cycles have been averaged over the same period. For models with several simulations, the error bars is the standard deviation of the simulations of that model. (b) Differences between the simulated annual cycles and the observed cycle [*Rothrock et al.*, 2008], expressed in terms of phase lag and difference of amplitude of the cycle. Positive phase lags correspond to a delay with respect to the observed cycle.

Table 2. Simulated Thinning and Speed Trends for the Periods 1980–2008 and 2020–2050 for Thickness and 1979–2007 and 2020–2050 for Sea Ice Speed[a]

Model	Run	1980–2008 Thickness Trend (+/−Error) (% per Decade)	2020–2050 Thickness Trend (+/−Error) (% per Decade)	1980–2008 September Thickness Trend (+/−Error) (% per Decade)	1979–2007 Speed Trend (+/−Error) (% per Decade)	2020–2050 Speed Trend (+/−Error) (% per Decade)
BCCR-BCM2.0	1	−3.7 (1.4)	−7.5 (1.5)	−5.6 (1.4)	1.2 (2.1)	3.3 (2.0)
CNRM-CM3	1	−3.4 (1.5)	−13.8 (1.7)	−6.0 (2.5)	−0.6 (1.8)	0.2 (1.9)
GISS aom	1	−2.0 (1.6)	−9.8 (1.5)	−3.0 (2.5)	−0.9 (2.2)	−0.4 (2.3)
	2	−4.7 (1.4)	−9.2 (1.5)	−3.8 (1.6)	2.4 (1.9)	1.6 (2.4)
GISS er	1	−2.5 (0.9)	−6.4 (1.2)	−3.0 (1.1)	5.0 (1.9)	6.5 (1.7)
	2	−3.1 (1.0)	−4.9 (1.2)	−3.6 (1.0)	2.5 (1.7)	3.0 (1.6)
	3	−0.9 (1.0)	−3.2 (1.1)	−0.6 (0.5)	−0.8 (1.7)	8.5 (1.7)
	4	−4.3 (1.0)	−2.5 (1.3)	−5.6 (0.5)	1.1 (1.8)	3.8 (1.6)
	5	−3.9 (1.0)	−1.8 (1.2)	−4.2 (0.8)	7.2 (1.9)	2.4 (1.6)
FGOALS-g1.0	1	−4.4 (0.2)	−8.8 (0.3)	−4.8(0.4)	7.4 (2.7)	8.2 (2.3)
INGV-SXG	1	−5.0 (1.9)	−21.6 (1.7)	−6.9 (3.9)	−0.9 (1.7)	−8.0 (1.9)
INM-CM3.0	1	−3.5(0.2)	−3.4(0.2)	−3.7(0.3)	-	-
MIROC3.2(Hires)	1	−9.8 (2.9)	−10.4 (3.3)	−18.6 (4.5)	−2.6 (2.0)	−6.6 (2.8)
MIUB-ECHO-G	1	−5.0 (1.2)	−5.8 (1.3)	−7.5 (2.6)	0.3 (1.4)	−1.5 (1.3)
	2	−1.4 (1.2)	−6.7 (1.3)	−0.7 (3.1)	−1.5 (1.4)	0.0 (1.4)
	3	−2.6 (1.1)	−3.3 (1.3)	−3.8 (2.6)	0.9 (1.3)	−0.7 (1.2)
ECHAM5/MPI-OM	1	−4.8 (0.6)	−16.0 (0.8)	−5.9 (1.7)	3.0 (2.0)	0.7 (2.1)
	3	−6.2 (0.7)	−15.5 (0.8)	−7.2 (1.9)	3.8 (2.0)	3.0 (1.7)
MRI-CGCM2.3.2	1	−5.4 (0.9)	−15.8 (0.7)	−5.5 (2.6)	−0.1 (1.6)	2.7 (1.6)
	2	−3.8 (1.0)	−9.4 (0.8)	−3.9 (3.3)	1.7 (1.6)	3.0 (1.5)
	3	−5.5 (0.7)	−15.7 (0.8)	−5.9 (2.0)	1.6 (1.5)	0.6 (1.4)
	4	−5.3 (0.7)	−15.5 (0.7)	−5.5 (2.0)	0.1 (1.6)	1.6 (1.4)
	5	−5.2 (0.7)	−5.5 (0.9)	−5.5 (1.5)	1.8 (1.5)	3.6 (1.6)
NCAR ccsm-PCM	1	−6.7 (0.7)	−10.7 (1.1)	−8.1 (2.0)	4.2 (2.2)	1.4 (2.8)
	2	−4.1 (0.9)	−12.2 (1.2)	−5.3 (2.7)	1.0 (1.8)	0.2 (1.7)
	5	−7.5 (0.6)	−13.3 (1.0)	−8.7 (1.4)	3.8 (2.0)	4.0 (2.7)
	6	−6.7 (0.8)	−16.6 (1.1)	−7.6 (2.8)	3.5 (2.0)	5.5 (2.7)
	7	−5.1 (0.8)	−7.4 (1.2)	−6.5 (2.5)	1.8 (2.1)	−0.8 (1.5)
UKMO-HadGEM1	1	−6.0 (1.4)	−10.6 (1.5)	−6.4 (2.9)	−0.6 (1.8)	−1.0 (1.7)
Ensemble mean		−4.6 (1.9)	−9.8 (5.1)	−5.6 (3.2)	1.6 (1.9)	1.6 (1.7)
Observations	Submarine and ICESat data [from *Kwok and Rothrock*, 2009]	−16.5 (7.0)		IABP Buoys [from *Rampal et al.*, 2009]	9.0 (1.9)	

[a]The trends are calculated from the 12 month running mean of the simulated monthly signals. Statistically significant positive trends (at a 95% confidence level), are in bold. Ice speed trend values and associated errors are computed using a weighted and tapered least squares method, i.e., taking into account the uncertainty and the temporal autocorrelation in the signals (see *Wunsch* [2006, p. 52] for details on this method).

consistently with the seasonal cycle of concentration and thickness [*Rothrock et al.*, 2008] since a thinner and less concentrated ice cover drifts faster. Most of the simulated speed annual cycles are lagged by about 2 to 4 months compared to observations (Figure 4). This means that the maximum speed is often obtained during late fall or winter, and the minimum in summer or early fall, in apparent contradiction with the corresponding simulated thickness cycles (Figure 2). To explain this unexpected behavior, we compared the simulated ice speed annual cycles to the corresponding annual cycles of the modeled wind speeds over the Arctic (Figure 5). These two cycles are in phase (±1 month) for all simulations, except for the BCCR-BCM2.0 and the FGOALS-g1.0 simulations (phase lag of more than 3 months) for which, instead, the ice speed and thickness annual cycles agree well (Figure 4c). All of this can therefore be interpreted as a lack of coupling between the ice state and ice kinematics in models: the annual cycle of the wind-forcing sets the ice speed annual fluctuations; that is, sea ice behaves as drifting freely, with a negligible influence of the internal stress term on ice motion, whatever the sophistication of the rheological model and particularly the parameterization of the ice

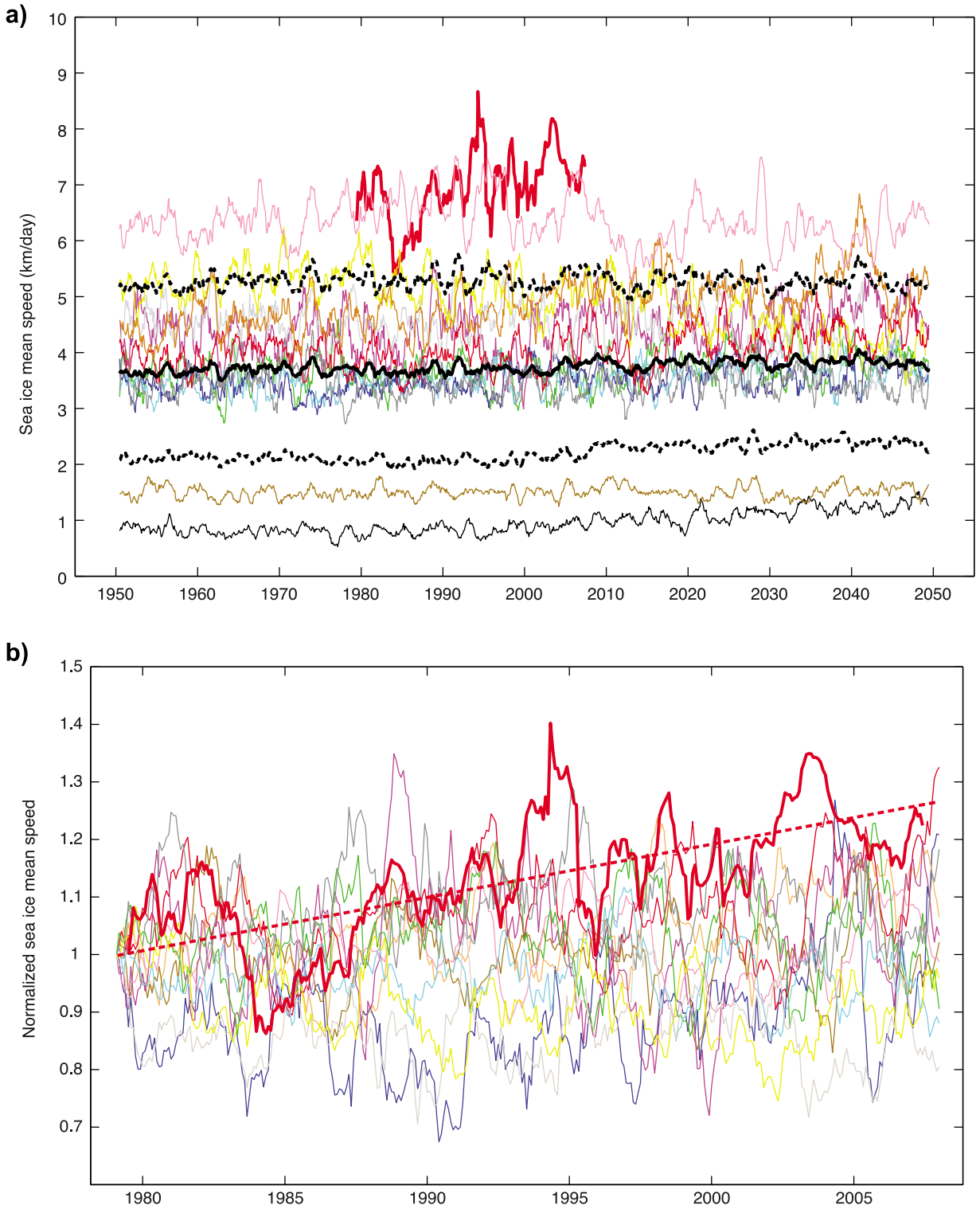

Figure 3. Simulated sea ice mean speed: comparison with observations. (a) Color codes are as in Figure 2. Thin colored lines, 12 month running mean of simulated sea ice speed spatially averaged over the central Arctic basin, 150 km from the coasts [see *Rampal et al.*, 2009, Figure 1], from 1950 to 2050. For clarity, only one simulation per model is shown. Thick black solid line, ensemble mean. Dashed black lines, ensemble mean ± one standard deviation. Thick red solid line, 12 month running mean of sea ice speed calculated from IABP buoy drift data from 1979 to 2007 [*Rampal et al.*, 2009]. (b) Same data zoomed over the period 1979–2007, and normalized by their value in 1979. Dashed red line, least squared fit (weighted by the uncertainty and with the correlation of the signal taken into account) of the buoy data, showing the positive trend over the period.

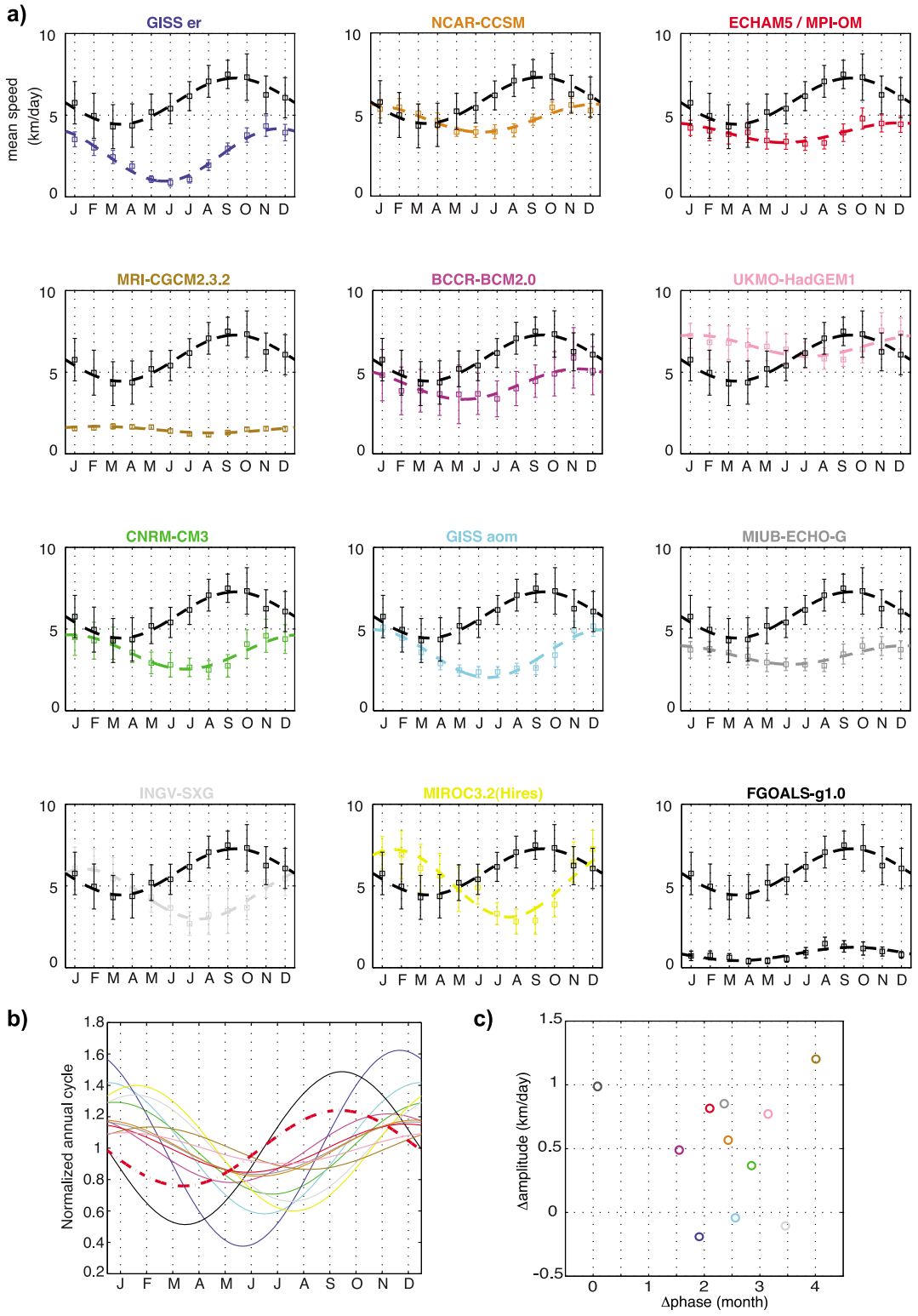

Figure 4. Annual cycle of spatially averaged sea ice speed. (a) Comparison of the simulated sea ice speed annual cycles with the cycle calculated from buoy data by *Rampal et al.* [2009], in dashed black line. The cycles have been averaged over the years 1979–2007. For models with several simulations, the error bars are the standard deviation of the simulations of that model. (b) The same cycles, normalized by their average amplitude. Dashed colored lines, simulations. Red dashed line, IABP buoy observations. (c) Differences between the simulated annual cycles and the observed cycle [*Rampal et al.*, 2009], expressed in terms of phase lag and difference of amplitude of the cycle. Positive phase lags correspond to a delay with respect to the observed cycle.

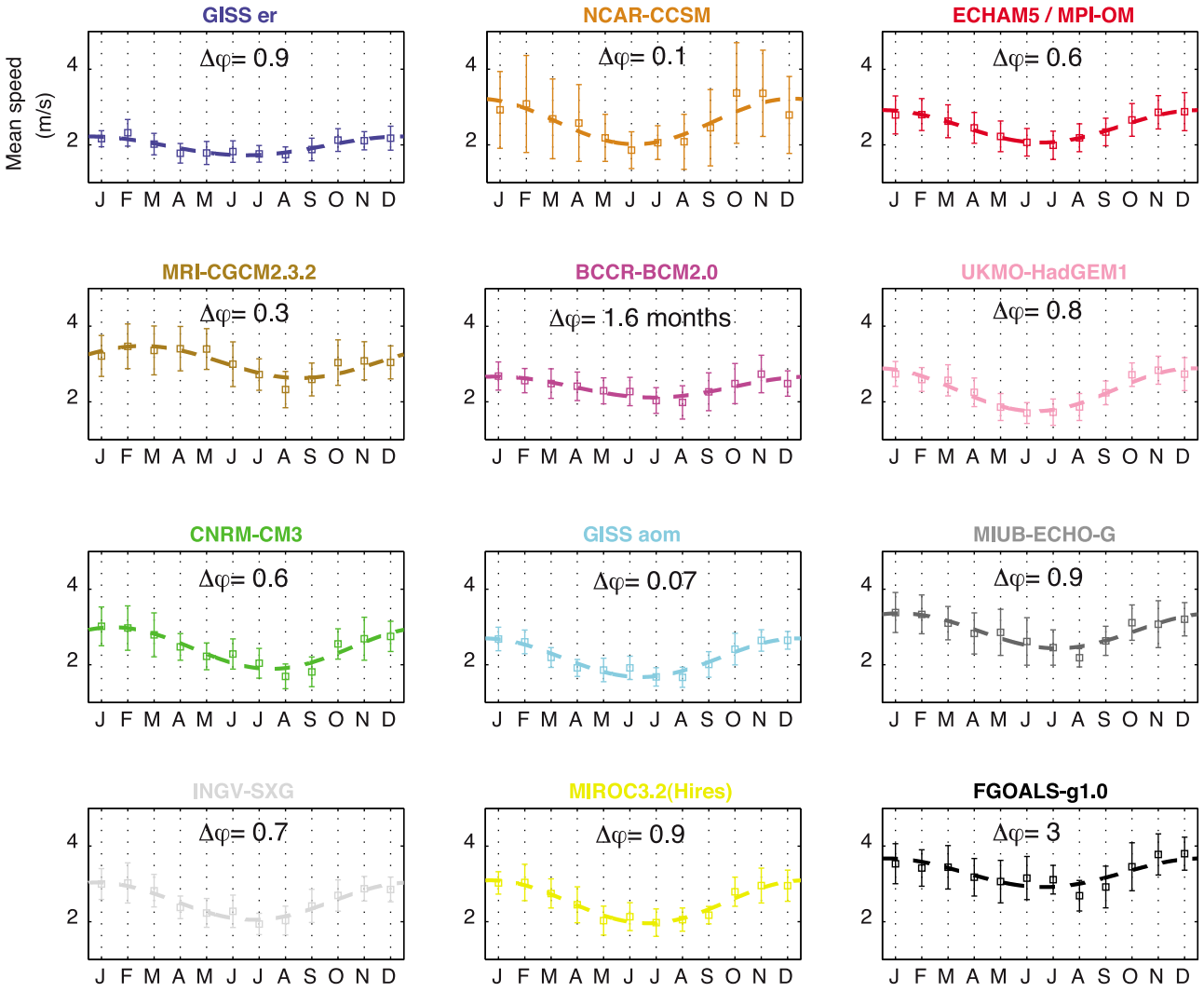

Figure 5. Annual cycle of spatially averaged simulated wind speed. Color codes are as in Figure 2. The wind speed values have been averaged over the region previously defined to calculate the sea ice speeds. The phase lag between the sea ice speed and wind speed cycles is indicated within each individual graph.

strength *P*. Consequently, the positive feedbacks between sea ice fracturing, deformation and drift in one hand, and sea ice melting, thinning, decreasing albedo and negative mass balance on the other hand, are at least poorly represented. As detailed below, a clear illustration of these shortcomings is sea ice export.

4.2. The Role of Sea Ice Export on Sea Ice Thinning and Decline

[18] As noted above, a possible effect of sea ice kinematics on sea ice mass balance and decline is through sea ice export, essentially at Fram Strait that accounts for roughly 90% of the total export according to the IPCC models evaluated here. Sea ice volume flux at a gate is a combination of ice velocity normal to the transect defining that gate, ice thickness and ice concentration at that gate. An estimation of effective volume fluxes therefore requires simultaneous in situ and/or satellite-derived records for these three quantities, which still remains challenging. Moreover, the volume flux calculation is strongly sensitive to the temporal and spatial resolution of these records, especially for ice thicknesses and velocities [e.g., *Spreen et al.*, 2009].

[19] Sea ice velocity variability through Fram Strait is positively correlated to cross-strait sea level pressure difference, i.e., to geostrophic winds [*Vinje*, 2001; *Widell et al.*, 2003]. NCEP/NCAR reanalysis data indicate a positive trend of about 10% per decade for this SLP difference over the period 1950–2000 [*Widell et al.*, 2003], therefore suggesting an associated positive trend on ice velocities across Fram Strait. Moreover, the accelerated kinematics over the last three decades within the Arctic Basin as the result of sea ice weakening induced by sea ice cover thinning [*Rampal et al.*, 2009] also argue for a similar trend across and south of Fram Strait. Although the IABP trajectories crossing the Fram Strait are too sparse to analyze this possibility, satellite-derived (SSM/I) velocity estimates showed a positive trend of 7% per decade for sea ice speeds in the region southward of that gate over 1979–2004, i.e., of the same order to the one observed within the basin (i.e., 9 (±1.9)% per decade) [*Rampal et al.*, 2009].

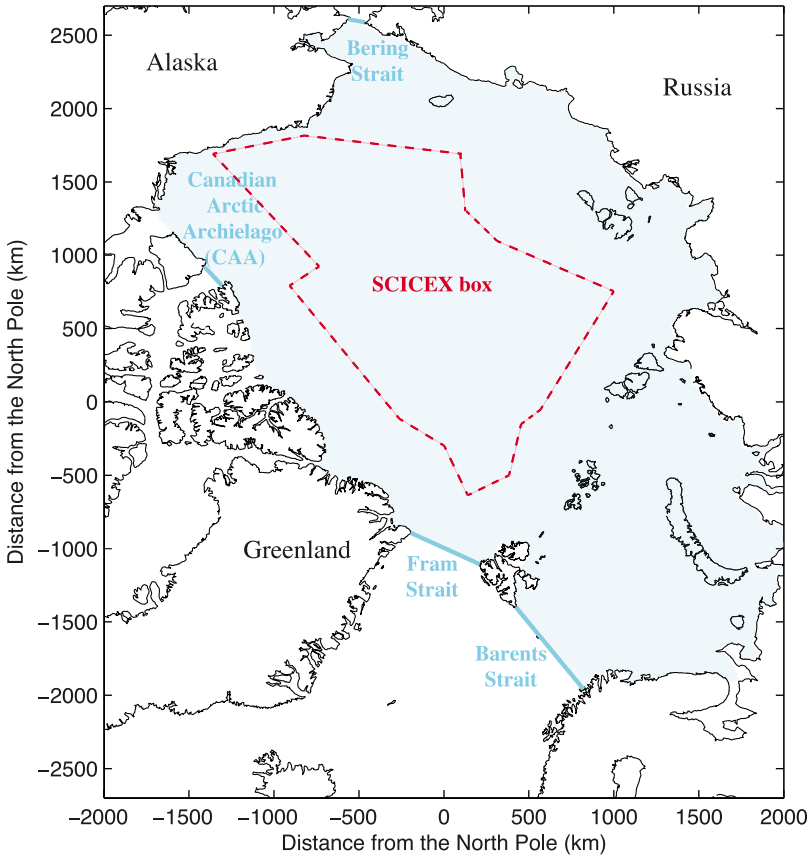

Figure 6. Map of the Arctic basin showing the domain (in light blue) used for our budget calculations. The transects considered as ice-exporting gates are shown in cyan blue, and correspond to the Fram Strait, Bering Strait, Barents Strait and Canadian Archipelago Strait. The SCICEX box region of *Rothrock et al.* [2008] is also shown (red dashed line).

[20] Several authors estimated area and/or volume export of sea ice from composite data sets [*Kwok*, 2009; *Kwok et al.*, 2004; *Spreen et al.*, 2009; *Vinje*, 2001]. For area fluxes, multidecadal trends vary from no significant trend [*Kwok*, 2009] to positive trends of few % per decade [*Kwok et al.*, 2004] superimposed to a strong interannual variability. Owing to the difficulty to obtain reliable thickness estimates, volume flux records are so far restricted to a few consecutive years, but a comparison of the available estimates argue for neither negative nor positive significant trend over the last two decades [*Spreen et al.*, 2009]. This absence of volume flux trend suggests that the observed negative trends on sea ice thickness and concentration have been compensated by a positive trend on ice velocities at gates [*Spreen et al.*, 2009]. Also, as the yearly averaged sea ice volume within the Arctic basin is decreasing, a constant outward volume flux in absolute value would mean an increasing relative impact on sea ice mass balance. Therefore, from a strictly kinematics point of view, observations argue for (1) accelerated ice drift across Fram Strait and (2) an increasing role of ice export on the observed negative mass balance of Arctic sea ice.

[21] Hereafter we analyze the sea ice velocities across Fram Strait in IPCC AR4 simulations and discuss the role of sea ice export on the negative mass balance of Arctic sea ice. In the next sections of this paper, we exclude two models from our calculations and discussions: the INM-CM3 model (which has no ice dynamics) and the FGOALS-g1.0 model (which has completely unrealistic ice thicknesses). To do our calculations, we define an Arctic domain (called *D* in the following) enclosed by transects across the Fram Strait, the Barents Sea, the Bering Strait and the Canadian Arctic Archipelago (Figure 6).

4.2.1. Sea Ice Speeds Across Fram Strait

[22] The ensemble mean of modeled sea ice speeds across Fram Strait shows a very slight evolution: a positive trend of about 1.3(±0.3)% per decade is found for the annual mean of the normal velocity component over the period 1950–2050 (Figure 7). The spread among simulations is large, with some negative trends. They range from −0.6% per decade for MIROC3.2(Hires) to 5.1% per decade for CNRM-CM3. For the period 1979–2007 over which most of the observations of sea ice fluxes have been reported (see above), this ensemble mean trend is even smaller with 0.7(±0.2)% per decade. Among simulations, the trends range from −0.9% per decade for BCCR-BCM2.0 to 2.1% per decade for NCAR-CCSM. No correlation is obtained between the sophistication of the rheological model and this trend on ice velocity at Fram Strait. This near absence of a significant trend, especially over the last three decades, could come from a too weak evolution for the cross-strait SLP difference, i.e., an inadequate atmospheric forcing of the models. We checked this hypothesis by computing the

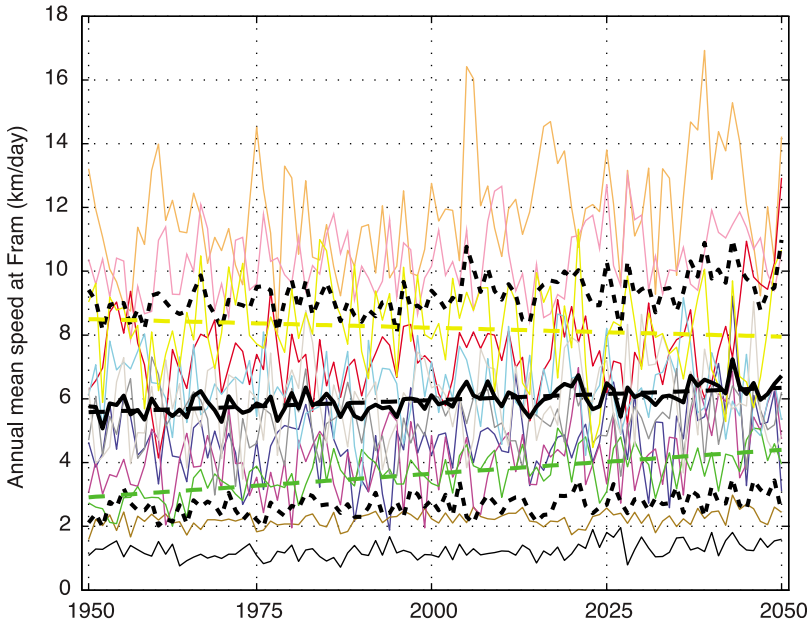

Figure 7. Simulated annual mean speed across Fram Strait. Color codes are as in Figure 2. The ensemble mean speed is drawn as the thick black line. Dispersion of the models is represented by the two dashed and black lines and corresponds to one standard deviation. Superimposed to models' series, the linear fit (in the least squared sense) of the ensemble mean is shown (thick black dashed line), as well as the linear fits that gave the smallest and largest trends, i.e., for MIROC3.2 (yellow) and CNRM-CM3 (green), respectively.

southward mean wind velocity at Fram Strait for each model, and found a ensemble mean positive trend of 6(±2)% per decade for the period 1979–2007, about the same order of magnitude as the trend estimated from the NCEP/NCAR reanalysis data for the period 1950–2000 [*Widell et al.*, 2003]. Therefore we believe that the absence of trend on ice speed at Fram Strait is a consequence of the lack of coupling between ice state and kinematics discussed above.

4.2.2. Role of Sea Ice Export on the Sea Ice Area, Volume, and Thickness Balances

[23] To compute the budgets of a quantity Q (volume, area or mean ice thickness) over the domain D, we use the simple following equation:

$$\frac{dQ}{dt} = T_Q - E_Q \tag{1}$$

where E_Q is a term of ice export out of the domain through the different gates and T_Q is the thermodynamic source term within the domain (i.e., the ice melt and/or growth). The monthly ice volume, ice area and mean ice thickness are computed over the domain D from

$$V(t) = \sum_D a \times h_{eff}(t) \tag{2}$$

$$A(t) = \sum_D a \times c(t) \tag{3}$$

$$\overline{h}(t) = \overline{h}_{eff}(t) = \frac{1}{N}\sum_D \frac{h_{eff}(t)}{c(t)} \tag{4}$$

respectively, where a is the grid cell area, h_{eff} is the monthly effective ice thickness (h_{eff} is the actual diagnostic variable given by the models, and is equal to the thickness over the ice covered portion of the grid cell multiplied by the ice-covered fraction of the cell $0 < c < 1$) and N is the number of grid cells in the domain D. We note that here the mean ice thickness is from the same calculation as in 3.1 with the difference that the spatial averaging is performed over the entire domain D instead of the SCICEX box domain. In (1), the monthly averaged tendencies $\frac{dQ}{dt}$ are computed from $V(t)$, $A(t$ or $\overline{h}(t)$. Volume and area export are computed at transects that are defined on the native model grids and thus that differ slightly among the models. However, the effects of these differences appear to be very small. The monthly integrated volume export E_V is computed using the mean velocity normal to each transect and the mean effective ice thickness obtained by averaging h_{eff} over the cells aligned to each transect. The monthly integrated area export E_A is computed using the mean velocity normal to each transect and the length l of each transect through which the ice is exported. l is computed for each transect as $\sum_{i=1:n} w_i \times c_i$ where w_i and c_i are the width and ice-covered fraction, respectively, of the cell i and n is the number of cells aligned to the transect. The monthly integrated thickness export $E_{\overline{h}}$ is defined as the thickness that, multiplied by the ice-covered area of the domain, returns the volume exported, i.e.:

$$E_{\overline{h}}(t) = \frac{E_V(t)}{A(t)} \tag{5}$$

[24] The thermodynamic sources terms T_V, T_A and $T_{\overline{h}}$ are then solved for as a residual from equation (1). Positive T_V,

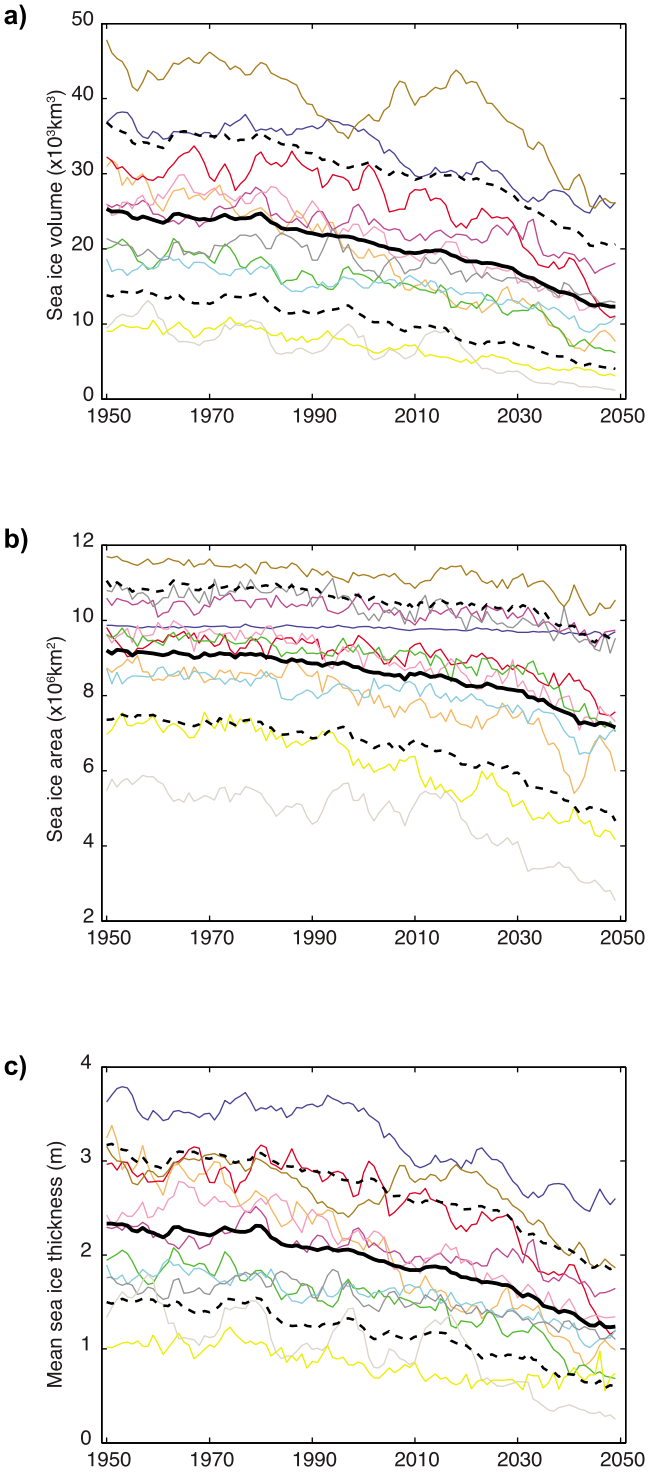

Figure 8. Simulated (a) sea ice volume, (b) area, and (c) mean thickness. Color codes are as in Figure 2. The calculations have been performed for the domain of Figure 6. Thin colored lines represent the 12 month running mean of the monthly time series. Thick black solid line, ensemble mean. Dashed black lines, ensemble mean ± one standard deviation.

T_A or $T_{\overline{h}}$ mean a net gain of ice mass, an increase of ice-covered area or a thickening of the ice cover over 1 month, respectively, resulting from thermodynamic processes.

[25] The near absence of positive trend for simulated ice velocities at export gates as shown in Figure 7 means that the underestimated but nevertheless negative trends on simulated thickness, area and volume within the basin (see Figure 8) will not be compensated. Therefore sea ice area and volume exports are expected to *decrease* in absolute value. This is indeed what we obtain for the IPCC models, with ensemble mean trends of −5.5(±0.6) and −2.2(±0.3)% per decade over the period 1950–2050 for volume and area, respectively (Figure 9). A positive trend on sea ice speed would contribute to reequilibrate this picture toward no (or positive) trend on the absolute ice volume (or area) exports through Fram Strait, and would give trends on ice flux in better agreement with the observations [*Kwok*, 2009; *Kwok et al.*, 2004; *Spreen et al.*, 2009]. To estimate the contribution of export to the net ice budget, we compute the fraction of total ice volume (and area) in the domain as well as the fraction of mean ice thickness that are exported each year between 1950 and 2050. The results are shown in Figure 10. The ensemble mean of the models is remarkably constant over the period. This means that sea ice export plays a negligible role on a negative balance of Arctic sea ice in IPCC AR4 simulations. To what extent could this explain the strong underestimation of Arctic sea ice thinning and decline?

4.2.3. Projected Arctic Sea Ice Thinning and Decline in Case of Accelerated Export

[26] We now explore further the impact of these models' deficiencies on Arctic sea ice balance and projections for the 21st century from the following calculation: over the period 1979–2007 and for each simulation, we applied a positive trend to the normal component of the ice velocities at gates. We recalculate sea ice area fluxes $E_A^*(t) = E_A(t) + E'_A(t)$ with these "trended" velocities but unchanged concentrations. In order to take into account that the enhanced area depletion induced by accelerated export would enhance new ice growth during winter (then acting as a negative feedback), we compute the respective climatology of each model (see Table 3). This climatology is defined as the mean annual cycle of the thermodynamic source term T_A of equation (1). From the annual cycle, we define for each model a "melt season" (MS) corresponding to the months when T_A is negative (i.e., when ice area is lost) and a "growth season" (GS) corresponding to the months when T_A is positive (i.e., when ice area is created). We assume that any additional export of area E'_A over a month of the GS is entirely balanced by an additional thermodynamic source term T'_A. On the contrary, an additional export of area during a month of the MS is definitively lost. Hence, the revised evolution of sea ice area $A^*(t)$ in the domain D can be expressed as a function of $A(t)$ as follows:

$$A^*(t) = A(t) - \sum_0^t E'_A(t|t \in MS) \tag{6}$$

[27] This way, we take into account, for ice area, of the negative feedback occurring mostly in winter and that implies

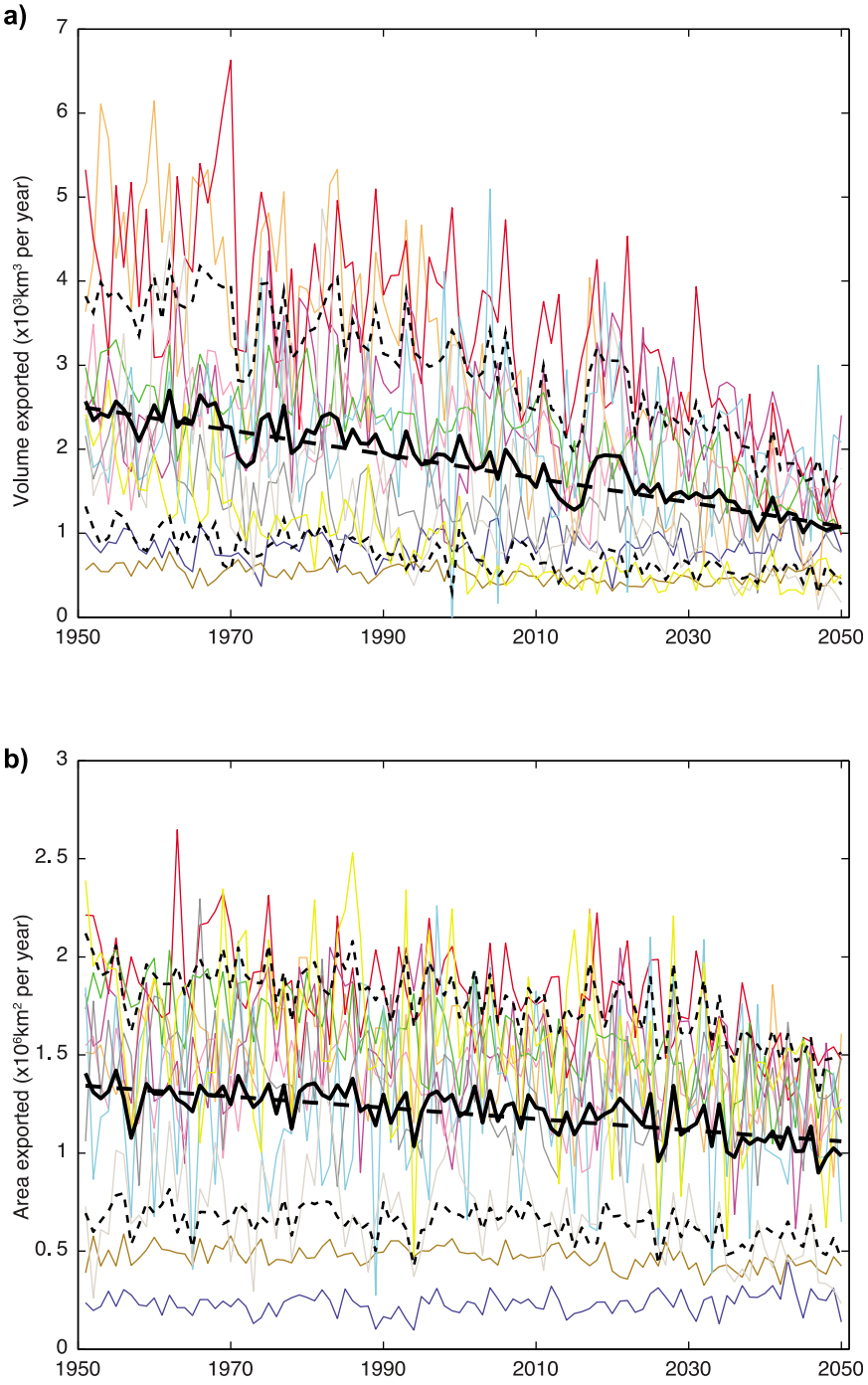

Figure 9. Simulated annual (a) sea ice volume and (b) area exports. Color codes are as in Figure 2. Annual exports are estimated from the monthly exports time series. Thick black solid line, ensemble mean. Dashed black lines, ensemble mean ± one standard deviation.

that an increasing ice export enhances a quasi simultaneous ice formation. On another hand, we neglect the fact that formation of open water area due to stronger export is recovered later in the year, e.g., at the refreezing period (November–December). However, we think that this assumption is reasonable as we checked that the modeled ice area export over the melting seasons is always small relatively to the yearly total export (i.e., of the order of 15% on average).

[28] We explored the impact of different trends on sea ice speeds on the revised evolution of sea ice area $A^*(t)$. For a positive trend of 9% at gates, i.e., equal to the drift acceleration found by *Rampal et al.* [2009] within the basin from buoy observations, 60% of the gap between the ensemble mean trend of models and the trend estimated over the domain D for sea ice areas derived from satellite passive microwave data for the period 1979–2007 (data available at ftp://sidads.colorado.edu/DATASETS/NOAA/G02135) is

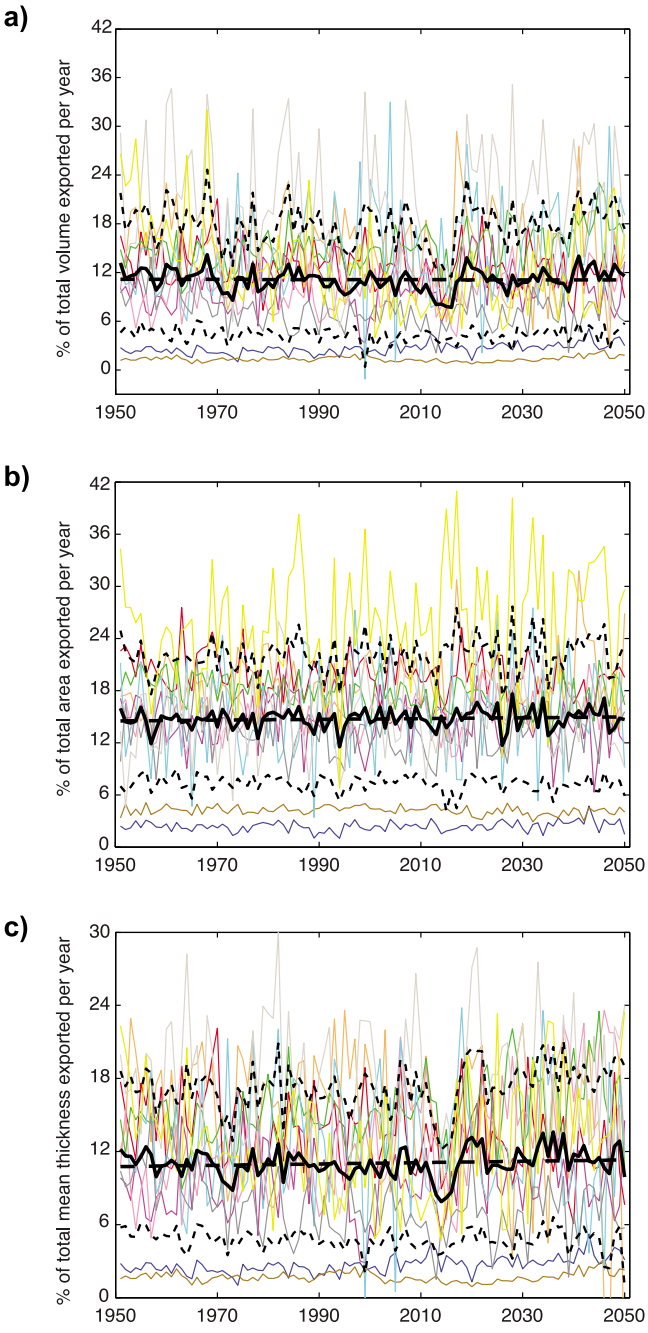

Figure 10. Fraction of total (a) ice volume, (b) area, and (c) mean thickness exported through the gates per year for the period 1950–2050. Color codes are as in Figure 2. Thick black solid line, ensemble mean. Dashed black lines, ensemble mean ± one standard deviation.

filled. A slightly larger ice speed acceleration of 12% per decade allows the ensemble mean trend to perfectly match the observed trend, either for the annual mean (Figure 11a), or the September minimum (Figure 11b).

[29] We extended our calculation to estimate the impact of such imposed sea ice speed trend at gates on the evolution of the mean ice thickness $\overline{h}$, and particularly to what extent increasing the ice export can reduce the mismatch between modeled and observed thinning trend (see section 3.1). In contrast to the area, we assume that a volume loss due to additional export is not restored via thermodynamic processes. Then we compute the revised evolution of mean thickness ar $\overline{h}^*(t)$ as

$$\bar{h}^*(t) = \frac{V^*(t)}{A^*(t)} \tag{7}$$

with

$$V^*(t) = V(t) - \sum_0^t \bar{h}_{trans}(t) E'_A(t) \tag{8}$$

where $\overline{h}_{trans}$ is the mean ice thickness averaged along each transect. This crude assumption means that if additional ice area export is compensated in winter by refreezing, the corresponding ice volume is neglected; that is, the associated ice thickness is small. Nevertheless, dividing by the revised area A^* in (7) allows taking into account in our estimation of a part of the thermodynamic negative feedback discussed above. We note that the modeled mean sea ice thickness negative thinning trend for the domain D (i.e., −4.3(±1.8)% per decade) is almost equal to the modeled trend found for the SCICEX box (i.e., −4.6(±1.9)% per decade, see section 3.1). Thus we can directly compare the modeled trend of $\overline{h}^*$ found for the domain D with the observations within the SCICEX region [*Kwok and Rothrock*, 2009]. Figure 12 shows the results. A trend of +9% per decade imposed on the ice speeds at the gates increases significantly the ensemble mean trend on mean ice thickness of models, which becomes about −13.4% per decade. The previous gap existing between modeled and observed trends is then reduced by 80%.

[30] Note that these simple calculations do not take into account the strengthening of the positive albedo feedback loop in summer through increasing fracturing, lead opening and ice concentration decline (see above). Therefore, although necessarily oversimplified, we believe that our calculation illustrates at least qualitatively the impact of inaccurate modeled kinematics onto present and future projections of sea ice thinning and mass balance.

5. Conclusions

[31] We analyzed the evolution of average Arctic sea ice thickness and drift speed as modeled by 13 IPCC-AR4

Table 3. Sea Ice Area Budget Climatology

Model	Melt ($\times 10^3$ km^2)	Growth ($\times 10^3$ km^2)	Melt Season (MS)
BCCR-BCM2.0	2677.7	4169.4	MJJAS
CNRM-CM3	4378.1	5967.7	JJA
GISS aom	4523.6	5760.7	MJJAS
GISS er	834.2	1066.3	JJAS
INGV-SXG	3976.3	4653.3	MJJA
MIROC3.2(Hires)	7369.9	8921.7	MJJAS
MIUB-ECHO-G	6689.8	8052.6	MJJA
ECHAM5/MPI-OM	2931.5	4725.1	MJJAS
MRI-CGCM2.3.2	2055.9	2521.2	AMJJAS
NCAR ccsm-PCM	4896.3	6360.3	AMJJAS
UKMO-HadGEM1	5273.9	6602.9	MJJA
Ensemble mean	4063.6	5263.1	MJJAS

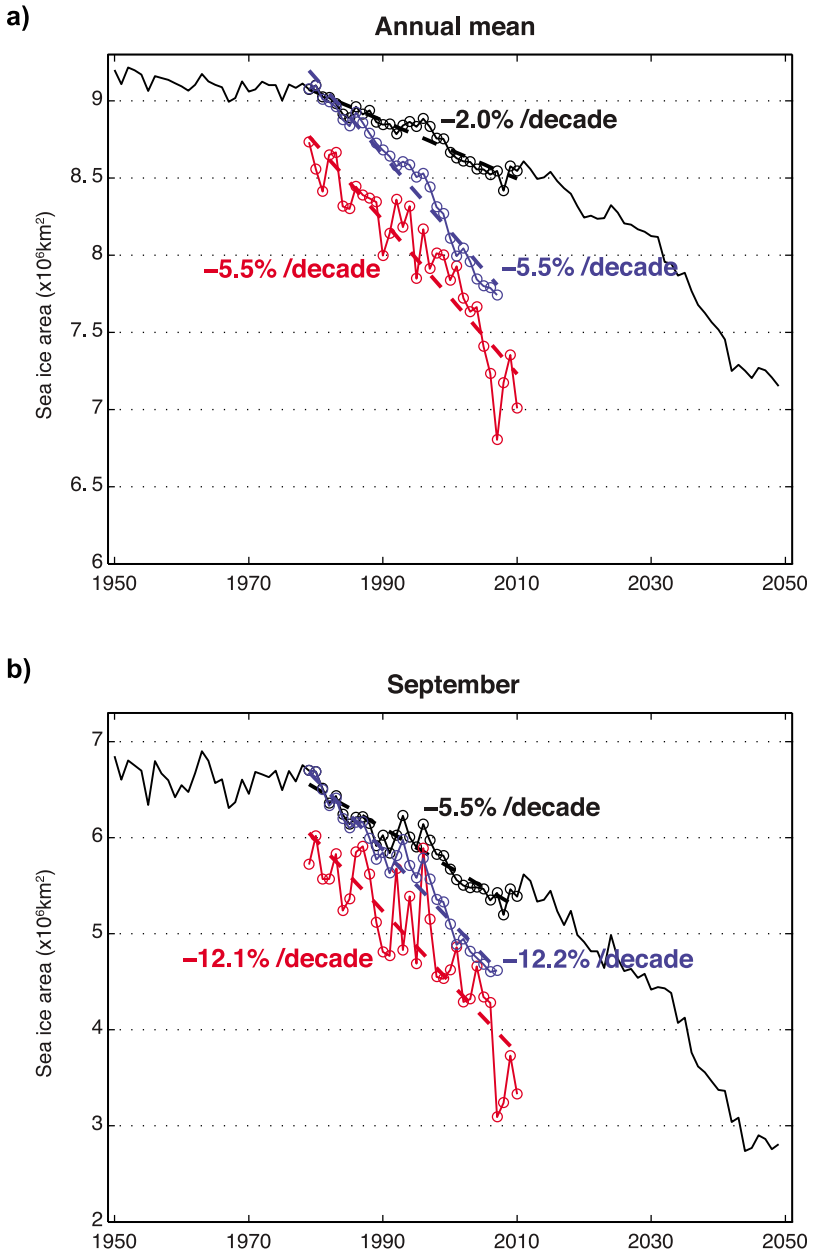

Figure 11. (a) Annual mean and (b) September sea ice area. For both Figures 11a and 11b, ensemble mean of the models is shown as the solid black line on which a linear fit of the data for the period 1979–2010 is superimposed (thick and dashed black lines). Satellite-derived estimates are plotted as red lines + circles, and the linear fits of these observations are drawn as the thick and dashed red lines. Blue circles show the obtained ice area if we impose a positive trend of 12% per decade on the ice speeds at gates over 1979–2007. This positive trend allows the ensemble mean trends on area, either for the annual mean or the September minimum, to perfectly match the observed trends (the linear fits shown on this figure are calculated in the least squared sense).

climate models from 1950 to 2050, and compared the trends to observations over the period 1979–2008. The main conclusions are:

[32] 1. Models underestimate the observed thinning trend by almost a factor 4 on average, i.e., in a way even more spectacular than they do for the sea ice extent decline. This underestimation of the thinning trend cannot be explained entirely by an underestimation of the decline of the perennial, thicker, ice-covered portion of the Arctic.

[33] 2. Models do not capture the acceleration of Arctic sea ice drift observed during the last decades.

[34] 3. An unexpectedly weak coupling between the ice state (thickness and concentration) and kinematics characterizes these IPCC simulations: for most models, ice drifts faster during the months it is thicker, in contradiction with observations, and models that show a stronger long-term thinning trend do not necessarily accelerate more. The absence of coupling between the ice state and ice kinematics

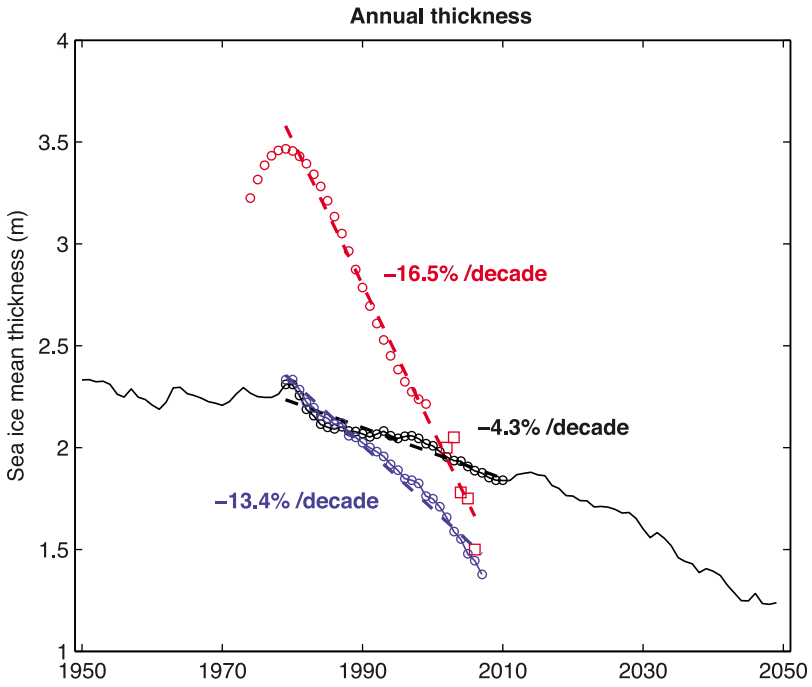

Figure 12. Annual sea ice mean thickness. Ensemble mean of the simulated sea ice mean thickness evolution is shown as the solid black line along with its respective linear fit for the period 1975–2010. Observations from *Kwok and Rothrock* [2009] are plotted as red circles (submarines data) and squares (ICESat data) along with their respective linear fit for the period 1975–2008. Blue circles show the obtained ensemble mean ice thickness if we imposed a positive trend of 9% per decade on the ice speeds at gates over the period 1979–2007. Such a positive trend reduces the gap between modeled and observed trend by 80% (the linear fits shown on this figure are calculated in the least squared sense).

in general means that modeled sea ice behaves as drifting freely, whatever the sophistication of the sea ice rheological model, and might explain partly why current climate models underestimate both the increasing kinematics and sea ice cover decline. Dedicated sensitivity modeling studies are needed to determine if these deficiencies could be improved from different parameterizations of current models, better numerical schemes, or would require a different rheological framework for sea ice [*Weiss et al.*, 2007; *Girard et al.*, 2011] in order to better represent the ice pack fracturing and, in turn, the ice drift properties. If increasing resolution may improve the forecast of sea ice thickness, possibly through a better representation of ocean heat transport [*Sewall*, 2008], it does not seem to improve the kinematics trends, at least within the rheological frameworks of the IPCC-AR4 models.

[35] 4. The simulated ice velocities across export gates (essentially, Fram Strait) show no significant long-term trend, with the consequence that sea ice volume fluxes from the Arctic basin are decreasing with time in absolute value, which is in disagreement with observations. Moreover, the relative percentage of simulated Arctic sea ice exported outward each year is remarkably constant, which means that in the models the ice export plays no role on the Arctic sea ice negative mass balance.

[36] 5. The IPCC deficiencies in reproducing the recent kinematics evolution is likely to have a significant impact on the simulated sea ice mass balance in the Arctic. As suggested by our simplistic evaluation, a (imposed) positive trend of 12% per decade on sea ice speeds at fluxgates, i.e., a value close to the observed drift acceleration within the Arctic basin, would significantly reduce the mismatch between modeled and observed sea ice area declining trends. Such accelerated export would also help the modeled ice cover thinning trend to be much closer to the observations.

[37] Therefore, this strong underestimation of sea ice thinning and drift acceleration in models would imply that former projections for an ice-free summer in the Arctic by 2100, based only on the comparison of simulated and observed sea ice extent reduction rates [*Arzel et al.*, 2006; *Boé et al.*, 2009b], are too conservative. This is reinforced by the fact that the current thinning trend is more than 40 years ahead of the ensemble mean forecast (Figure 1), whereas the fraction of the ocean covered by ice is highly sensitive to ice thickness changes [*Lindsay et al.*, 2009].

[38] **Acknowledgments.** P.R. is supported in part through a JPL-MIT Strategic University Research Partnership grant and the Estimating the Circulation and Climate of the Ocean (ECCO) project. We acknowledge the modeling groups, the Program for Climate Model Diagnosis and Intercomparison (PCMDI) and the WCRP's Working Group on Coupled Modeling (WGCM), for their roles in making available the WCRP CMIP3 multimodel data set. Support of this data set is provided by the Office of Science, U.S. Department of Energy. We deeply thank the two anonymous reviewers for their suggestions that help us improve the manuscript. We also thank D. Salas Mélia (Meteo France), G. Forget (MIT), P. Heimbach (MIT), and A. T. Nguyen (MIT) for their interesting suggestions.

References

Arzel, O., T. Fichefet, and H. Goosse (2006), Sea ice evolution over the 20th and 21st centuries as simulated by current AOGCMs, *Ocean Modell.*, *12*(3–4), 401–415, doi:10.1016/j.ocemod.2005.08.002.

Boé, J. L., A. Hall, and X. Qu (2009a), Current GCMs' unrealistic negative feedback in the Arctic, *J. Clim.*, *22*(17), 4682–4695, doi:10.1175/2009JCLI2885.1.

Boé, J. L., A. Hall, and X. Qu (2009b), September sea-ice cover in the Arctic Ocean projected to vanish by 2100, *Nat. Geosci.*, *2*(5), 341–343, doi:10.1038/ngeo467.

Comiso, J. C., C. L. Parkinson, R. Gersten, and L. Stock (2008), Accelerated decline in the Arctic sea ice cover, *Geophys. Res. Lett.*, *35*, L01703, doi:10.1029/2007GL031972.

Eisenman, I., N. Untersteiner, and J. S. Wettlaufer (2007), On the reliability of simulated Arctic sea ice in global climate models, *Geophys. Res. Lett.*, *34*, L10501, doi:10.1029/2007GL029914.

Feltham, D. (2008), Sea ice rheology, *Annu. Rev. Fluid Mech.*, *40*, 91–112, doi:10.1146/annurev.fluid.40.111406.102151.

Flato, G. M., and W. D. Hibler (1992), Modeling pack ice as a cavitating fluid, *J. Phys. Oceanogr.*, *22*(6), 626–651, doi:10.1175/1520-0485(1992)022<0626:MPIAAC>2.0.CO;2.

Girard, L., S. Bouillon, J. Weiss, D. Amitrano, T. Fichefet, and V. Legat (2011), A new modelling framework for sea-ice mechanics based on elasto-brittle rheology, *Ann. Glaciol.*, *52*(57), 123–132, doi:10.3189/172756411795931499.

Gorodetskaya, I. V., L. B. Tremblay, B. Liepert, M. A. Cane, and R. I. Cullather (2008), The influence of cloud and surface properties on the Arctic Ocean shortwave radiation budget in coupled models, *J. Clim.*, *21*(5), 866–882, doi:10.1175/2007JCLI1614.1.

Haas, C., A. Pfaffling, S. Hendricks, L. Rabenstein, J. L. Etienne, and I. Rigor (2008), Reduced ice thickness in Arctic transpolar drift favors rapid ice retreat, *Geophys. Res. Lett.*, *35*, L17501, doi:10.1029/2008GL034457.

Hakkinen, S., A. Proshutinsky, and I. Ashik (2008), Sea ice drift in the Arctic since the 1950s, *Geophys. Res. Lett.*, *35*, L19704, doi:10.1029/2008GL034791.

Hibler, W. D. I. (1979), A dynamic thermodynamics sea ice model, *J. Phys. Oceanogr.*, *9*, 815–846, doi:10.1175/1520-0485(1979)009<0815:ADTSIM>2.0.CO;2.

Hunke, E. C., and J. K. Dukowicz (1997), An elastic-viscous-plastic model for sea ice dynamics, *J. Phys. Oceanogr.*, *27*(9), 1849–1867, doi:10.1175/1520-0485(1997)027<1849:AEVPMF>2.0.CO;2.

Kwok, R. (2009), Outflow of Arctic Ocean sea ice into the Greenland and Barents Seas: 1979–2007, *J. Clim.*, *22*(9), 2438–2457, doi:10.1175/2008JCLI2819.1.

Kwok, R., and D. A. Rothrock (2009), Decline in Arctic sea ice thickness from submarine and ICESat records: 1958–2008, *Geophys. Res. Lett.*, *36*, L15501, doi:10.1029/2009GL039035.

Kwok, R., G. F. Cunningham, and S. S. Pang (2004), Fram Strait sea ice outflow, *J. Geophys. Res.*, *109*, C01009, doi:10.1029/2003JC001785.

Kwok, R., G. F. Cunningham, M. Wensnahan, I. Rigor, H. J. Zwally, and D. Yi (2009), Thinning and volume loss of the Arctic Ocean sea ice cover: 2003–2008, *J. Geophys. Res.*, *114*, C07005, doi:10.1029/2009JC005312.

Kwok, R., L. T. Pedersen, P. Gudmandsen, and S. S. Pang (2010), Large sea ice outflow into the Nares Strait in 2007, *Geophys. Res. Lett.*, *37*, L03502, doi:10.1029/2009GL041872.

Lemke, P., et al. (2007), Observations: Changes in snow, ice and frozen ground, in *Climate Change 2007: The Physical Science Basis. Contribution of Working Group I to the Fourth Assessment Report of the Intergovernmental Panel on Climate Change*, edited by S. Solomon et al., Cambridge Univ. Press, Cambridge, U. K.

Lindsay, R. W., J. Zhang, A. Schweiger, M. Steele, and H. Stern (2009), Arctic sea ice retreat in 2007 follows thinning trend, *J. Clim.*, *22*, 165–176, doi:10.1175/2008JCLI2521.1.

Lipscomb, W. H., E. Hunke, W. Maslowski, and J. Jakacki (2007), Ridging, strength and stability in high-resolution sea ice models, *J. Geophys. Res.*, *112*, C03S91, doi:10.1029/2005JC003355.

Maslanik, J. A., C. Fowler, J. Stroeve, S. Drobot, J. Zwally, D. Yi, and W. Emery (2007), A younger, thinner Arctic ice cover: Increased potential for rapid, extensive sea-ice loss, *Geophys. Res. Lett.*, *34*, L24501, doi:10.1029/2007GL032043.

Nghiem, S. V., I. G. Rigor, D. K. Perovich, P. Clemente-Colon, J. W. Weatherly, and G. Neumann (2007), Rapid reduction of Arctic perennial sea ice, *Geophys. Res. Lett.*, *34*, L19504, doi:10.1029/2007GL031138.

Rampal, P., J. Weiss, and D. Marsan (2009), Positive trend in the mean speed and deformation rate of Arctic sea ice: 1979–2007, *J. Geophys. Res.*, *114*, C05013, doi:10.1029/2008JC005066.

Rothrock, D. A., D. B. Percival, and M. Wensnahan (2008), The decline in arctic sea-ice thickness: Separating the spatial, annual, and interannual variability in a quarter century of submarine data, *J. Geophys. Res.*, *113*, C05003, doi:10.1029/2007JC004252.

Salas Mélia, D. (2002), A global coupled sea ice–ocean model, *Ocean Modell.*, *4*, 137–172, doi:10.1016/S1463-5003(01)00015-4.

Serreze, M. C. (2009), Arctic climate change: Where reality exceeds expectations, *Arctic*, *13*(1), 1–4.

Serreze, M. C., and J. A. Francis (2006), The arctic amplification debate, *Clim. Change*, *76*(3–4), 241–264, doi:10.1007/s10584-005-9017-y.

Serreze, M. C., M. M. Holland, and J. Stroeve (2007), Perspectives on the Arctic's shrinking sea-ice cover, *Science*, *315*, 1533–1536, doi:10.1126/science.1139426.

Sewall, J. O. (2008), Model resolution influence on simulated sea ice decline, *Cryosphere Discuss.*, *2*, 759–776, doi:10.5194/tcd-2-759-2008.

Skyllingstad, E. D., C. A. Paulson, and D. K. Perovich (2009), Simulation of melt pond evolution on level ice, *J. Geophys. Res.*, *114*, C12019, doi:10.1029/2009JC005363.

Spreen, G., S. Kern, D. Stammer, and E. Hansen (2009), Fram Strait sea ice volume export estimated between 2003 and 2008 from satellite data, *Geophys. Res. Lett.*, *36*, L19502, doi:10.1029/2009GL039591.

Stroeve, J., M. M. Holland, W. Meier, T. Scambos, and M. Serreze (2007), Arctic sea ice decline: Faster than forecast, *Geophys. Res. Lett.*, *34*, L09501, doi:10.1029/2007GL029703.

Tremblay, L. B., M. M. Holland, I. V. Gorodetskaya, and G. A. Schmidt (2007), An ice-free Arctic? Opportunities for computational science, *Comput. Sci. Eng.*, *9*(3), 65–74, doi:10.1109/MCSE.2007.45.

Tschudi, M., C. Fowler, J. Maslanik, and J. Stroeve (2010) Tracking the movement and changing surface characteristics of arctic sea ice, *IEEE J. Sel. Top. Appl. Earth Obs. Remote Sens.*, *3*, 536–540.

Vavrus, S., D. Waliser, A. Schweiger, and J. Francis (2009), Simulations of 20th and 21st century Arctic cloud amount in the global climate models assessed in the IPCC AR4, *Clim. Dyn.*, *33*(7–8), 1099–1115, doi:10.1007/s00382-008-0475-6.

Vinje, T. (2001), Fram strait ice fluxes and atmospheric circulation: 1950–2000, *J. Clim.*, *14*(16), 3508–3517, doi:10.1175/1520-0442(2001)014<3508:FSIFAA>2.0.CO;2.

Weiss, J., E. M. Schulson, and H. L. Stern (2007), Sea ice rheology from in-situ, satellite and laboratory observations: Fracture and friction, *Earth Planet. Sci. Lett.*, *255*, 1–8, doi:10.1016/j.epsl.2006.11.033.

Widell, K., S. Osterhus, and T. Gammelsrod (2003), Sea ice velocity in the Fram Strait monitored by moored instruments, *Geophys. Res. Lett.*, *30*(19), 1982, doi:10.1029/2003GL018119.

Winton, M. (2008), Sea ice-albedo feedback and Nonlinear Arctic climate change, in *Geophys. Monogr. Ser.*, vol. 180, *Arctic Sea Ice Decline: Observations, Projections, Mechanisms, and Implications*, edited by E. T. DeWeaver, C. M. Bitz, and L.-B. Tremblay, pp. 111–131, AGU, Washington, D. C.

Wunsch, C. (2006), *Discrete Inverse and State Estimation Problems*, Cambridge Univ. Press, Cambridge, U. K.

Zhang, J., D. Rothrock, and M. Steele (2000), Recent changes in arctic sea ice: The interplay between ice dynamics and thermodynamics, *J. Clim.*, *13*(17), 3099–3114, doi:10.1175/1520-0442(2000)013<3099:RCIASI>2.0.CO;2.

J.-M. Campin, Earth, Atmospheric and Planetary Science, Massachusetts Institute of Technology, 77 Massachusetts Ave., Cambridge, MA 02139, USA.

C. Dubois, Centre National de Recherches Météorologiques, 42 Ave. G. Coriolis, F-31057 Toulouse, France.

P. Rampal and J. Weiss, Laboratoire de Glaciologie et Géophysique de l'Environnement, CNRS/Université Joseph Fourier, 54 rue Molière, BP 96, F-38402 St Martin d'Hères, France. (rampal@mit.edu)